Met. Mater. Int., Vol. 18, No. 1 (2012), pp. 121~128
doi: 10.1007/s12540-012-0014-1 Published 27 February 2012

Nanocrystalline Copper Coatings Produced by Cold Spraying

Jingchun Liu[1], Hua Cui[2], Xianglin Zhou[1,*], Xiangkun Wu[1], and Jishan Zhang[1,*]

[1]State Key Laboratory for Advanced Metals and Materials,
University of Science and Technology Beijing, Beijing, 100083, China
[2]School of Materials Science and Engineering, University of Science and Technology Beijing,
Beijing, 100083, China

(received date: 12 November 2010 / accepted date: 30 December 2010)

Copper powder was cryomilled for 12 hours to achieve particle size in the range of 2 μm to 25 μm, which powder was subsequently used as feedstock for the deposition of nanocrystalline (nc) Cu coating via cold spraying. The as-milled copper powder was characterized by X-ray diffraction (XRD), scanning electron microscopy (SEM) and high resolution transmission electron microscopy (HRTEM). The particle size of the cryomilled Cu powder was detected by laser scattering. The microstructure of the coating was analyzed using SEM and scanning transmission electron microscopy (STEM). The XRD and HRTEM analysis showed that the grain size of the cryomilled Cu powder was about 5 to 40 nm. This nanoscale structure was retained after the cold spraying. The nanoindentation analysis showed that the nc Cu coating hardness value reached 3.3 GPa, which was higher than that of its coarse grained counterpart.

Key words: nanostructured materials, coating, microstructure, indentation, cold spraying

1. INTRODUCTION

Nanocrystalline materials, characterized by a microstructural length scale of 1 to 100 nm, have spurred considerable scientific attention and technological interest because the small grain can exhibit peculiar and interesting mechanical and physical properties, e.g. increased mechanical strength, enhanced diffusivity, higher specific heat and electrical resistivity compared to these materials' conventional coarse grained counterparts [1,2]. Numerous techniques can be used to produce nanostructured materials, but most of these techniques are limited to synthesis in small quantities [1]. The cryomilling technique has been proven to be a versatile technique for the fabrication of of nanocrystalline powders in quantities that are sufficient for industrial application [3,4]. Cryomilling is a mechanical milling technique in which powders are milled in a slurry formed with milling balls and a cryogenic liquid. During the process, the welding and fracturing of particles leads to severe plastic deformation. The continuous process produces micron size agglomerates with a nanoscale structure. The unique advantages of cryomilling include: reduced oxygen contamination from the atmosphere; faster convective heat transfer from the particles to the cryogenic media, which results in a lower particle temperature in favor of fracturing over welding of ductile materials during the milling process; reduced milling time to achieve nanograins (hindering of microstructural recovery due to low temperature); and higher thermal stability of the material, attributed to pinning effects arising from the presence of dispersoids formed during cryomilling [5].

Cold spray has come to be understood, within the larger family of thermal spray processes, as a materials deposition process in which relatively small particles (ranging in size from approximately 1 to 50 μm in diameter), at temperatures lower than the melting point of the powder material, are accelerated to high velocities (typically 300 to 1200 m/s), and subsequently impact, deform plastically and then mechanically and/or metallurgically bond to the substrate to form a uniform coating [6,7]. Recently, a thermal boost-up zone (TBZ) based on experimental and finite element simulation studies was proposed to estimate the occurrence of adiabatic shear instability and thus critical velocity [8]. This model can interpret the thin molten layer localized in the interface, which may result in reliable metallurgical bonding [8-10]. Therefore, the TBZ model seems to be relatively reasonable at present. The cold spray, as opposed to the sprays found in thermal spraying processes (e.g., high velocity oxygen-fuel (HVOF) spray, flame spray and plasma spray), has a unique advantage in that there is the possibility of retaining the microstructure and the mechanical and chemical properties of the particle feedstock. The cold spray method has been

*Corresponding author: bkdzxl@sina.com, zhangjs@skl.ustb.edu.cn

used to deposit many types of materials including pure metals [11-14], intermetallics [15], amorphous alloys [16-19], and composite materials [20-22]. Recently, nc materials, including aluminum alloys [23-26], Fe-Si [27], pure nickel [28], WC/Co [29,30], copper alumina composite materials [31], carbon nanotube reinforced aluminum composite materials [32], and carbon nanotube reinforced copper composites [33], were also prepared via the cold spray process, demonstrating the potential of the process to produce nc coatings and structures. The combination of two processing techniques, cryomilling and the cold spray process, provides the opportunity to synthesize nc deposits with grain sizes on the order of tens of nanometers [23-26,28].

The main objectives of the present study are to produce nanocrystalline copper coatings via cold spray technology. The microstructure and preliminary mechanical properties of the nanocrystalline copper coatings were investigated.

2. EXPERIMENTAL PROCEDURE

2.1. Powder preparation

Commercially available atomized Cu powder (99.81 wt.% purity, –45 μm, GRIPM Advanced Materials Co., Ltd., Beijing, China) was used in the present study. The copper powder was mechanically milled at the rate of 200 rpm in a modified attritor mill for 12 hours under a liquid nitrogen environment, with gas continuously introduced into the vessel during milling to ensure complete immersion of the powders and the balls. Stainless steel balls of 6.4 mm in diameter were used as the grinding media, and the ball-to-powder weight ratio was 30:1. The temperature in the vial was between –160 ℃ and –193 ℃. The process details on the cryomilling can be found elsewhere in the literatures [34-36].

2.2. Cold spray apparatus and coating preparation

The cold spray system developed at the University of Science and Technology Beijing was used to produce nanostructured copper coatings. The system includes gas pressure regulators, a gas preheater, a high pressure powder feeder, a spray gun and motion control equipment such as an X-Y-Z coordinate. Figure 1 shows a schematic diagram of the cold spray facility. The carrier gas is connected to a commercially available powder feeder (UNIQUECOAT, model SSP-100) and entrains the powder particles into the main flow. The spray gun mainly consists of a gas pre-chamber and a convergent-divergent accelerating nozzle. The powder is fed axially into the upstream of the nozzle from the back of the gun and the accelerating gas is introduced from the gas inlet into the pre-chamber. The gas temperature and pressure in the pre-chamber are measured via the thermocouple and pressure gauge mounted on the spray gun. The substrate holder is mounted on a motorized X-Y traverse system equipped with a computer controlled variable velocity positioning system. The cryomilled powder was sprayed onto a polished 6061 aluminum substrate using the cold spraying process. Nitrogen gas at a temperature of about 300 ℃ was used as the driving and carrier gas. The accelerating gas stagnation pressure was set at 2.0 MPa and the powder carrier gas was kept 0.2 MPa higher than that of the accelerating gas in order to facilitate the injection of the powder into the jet. The substrate was moved at a speed of 5 mm/s relative to the rest gun, under the nozzle jet, to build up the thickness of the coating in one pass. The stand-off distance is 10 mm. During the preparation of the conventional Cu coating, the accelerating gas stagnation pressure was set at 1.5 MPa. The substrate was manipulated at the speed of 10 mm/s relative to the rest gun, and the stand-off distance was 20 mm.

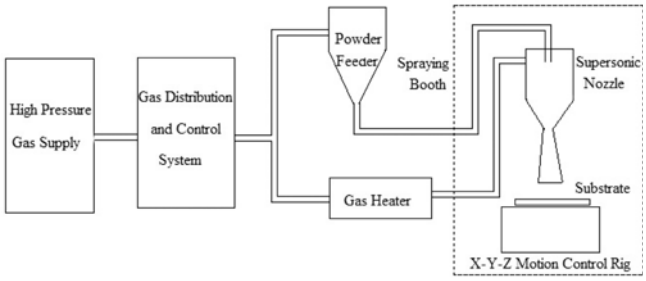

Fig. 1. Schematic of the cold spray facility.

2.3. Powder and coating characterization

The morphology and microstructure observations of the powders were conducted using a ZEISS SUPRA55 field emission scanning electron microscope (SEM) equipped with an energy dispersion spectroscope (EDS). The particle size distribution was determined using a SEISHIN LMS-30 laser scattering particle size analyzer (PSA) with analytical pure ethanol as the dispersant. Microstructure analysis of the as-milled powder was performed using a JEM-2010 high resolution transmission electron microscope (HRTEM) with an acceleration voltage of 200 kV. The HRTEM sample of the powders was prepared using the carbon grid method [5]. XRD analysis was performed in the 2θ range of 10 to 100 using Cu K_α (λ=0.15406 nm) radiation in a PHILIPS APD-10 diffractometer equipped with a graphite monochromator. After the component of $K_{\alpha 2}$ was corrected, the peak data, e.g. the full width at half maximum of the diffraction peaks, were measured using a software package in the diffractometer. In the present study, fully annealed pure copper powders were selected as standard samples for the determination of instrumental broadening. The calculation of grain sizes based on the XRD data was conducted by the Integral Breadth method, assuming a Cauchy-Gaussian profile of the reection [37,38]:

$$\frac{(\delta 2\theta)^2}{\tan^2\theta_0} = \frac{K\lambda}{L}\left(\frac{\delta 2\theta}{\tan\theta_0 \sin\theta_0}\right) + 16e^2 \quad (1)$$

in which K is a constant taken as 1, where θ_0 is the position

of the analyzed peak maximum, λ is the X-ray wave length, L is the crystallite size, e is the maximum strain, and $\delta 2\theta = B(1-b^2/B^2)$; b and B are the breadths in radians of the same peak in the reference and experimental patterns, respectively. Any available order of a given reflection may be used to construct a linear plot of $(\delta 2\theta)^2\theta_0$ against $(\delta 2\theta)/(\tan\theta_0\sin\theta_0)$. From the slope, λ/L, and ordinate intercept, $16e^2$, the crystallite size, L, and strain, e, may be determined.

The cross-sections of the coatings were also analyzed by SEM. Prior to SEM imaging, the test samples for cross-sectional observation were sectioned and polished using standard metallographic techniques. A Philips/FEI Tecnai F20 scanning transmission electron microscope (STEM) operating at an accelerating voltage of 200 kV was used to study the microstructure of the coating. The samples for TEM were in the form of a 3 mm disc, and were punched from a coating less than 50 μm thick prepared by grinding on a 2000 grit abrasive paper. The final thinning was carried out by ion-beam thinning at a current of 0.5 mA and an inclination angle of 12° (Model 691 PIPS, Gatan, Inc., CA, USA).

To investigate the mechanical properties of the coatings, nanoindentation studies were conducted in an MTS Nanoindenter DCM (Berkovich, Oak Ridge, TN, indenter) on the cross section of the sprayed coatings. Nanoindentation tests at constant strain rates in ranges of about 10^{-2}~10^{-3} s^{-1} were preformed for the nc Cu coatings and conventional Cu coatings. Prior to the nanoindentation tests, the cross sections of the sprayed coatings were ground (1200, 1500, 2000 grit) and polished (2.5, 1.5, 1, 0.5 μm diamond slurry). The continuous stiffness measurement (CSM) approach was used to determine the hardness test values from the nanoindentation tests [39,40]. An indentation depth of 300 nm was employed in this study. The reported values are the average of 6 indentations for each sample.

3. RESULTS AND DISCUSSION

3.1. Powder characterization

The morphology of the atomized and cryomilled powders is shown in Fig. 2. The morphology of the atomized powder was nearly spherical, conforming to what is usually seen in water-atomized powder (Fig. 2(a)); on the other hand, cryomilling of the water atomized powder led to the formation of irregular and flake-shaped agglomerates, as shown in Fig. 2(b). This was a result of the continuous flattening, welding and fracturing of the powder particles during the cryomilling process [3,4]. The Cu powder was cryomilled for 12 hours to generate flake-like powder particles.

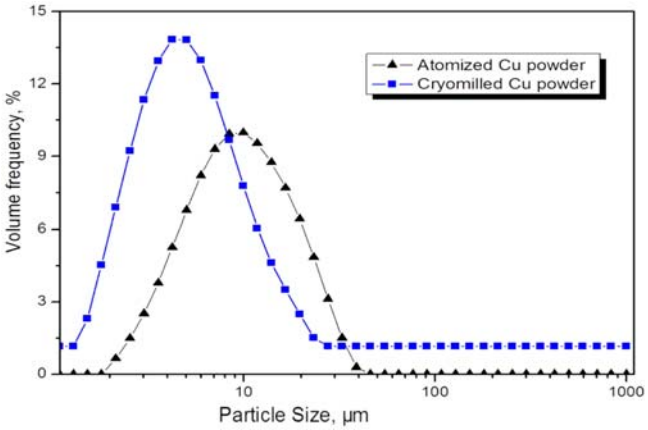

Fig. 3. Particle size distribution of Cu powders before and after cryomilling.

The measured particle size distributions are shown in Fig. 3. The mean particle size of the atomized Cu powders was 10 μm. The particle size of the cryomilled Cu powder was in the range of 2 μm to 25 μm. The particle size distribution curve of atomized Cu powders was a little broader than that of cryomilled Cu powders, as shown in the graph; the average size of the original powders was a little larger than that of the cryomilled powders.

Figure 4 shows the XRD patterns of the cryomilled Cu powders. It can be seen that the intensity of the Cu peak in the XRD patterns decreased quickly after 3 hours. In addition, the broadening of the Cu peaks can be clearly observed. The calculation of grain sizes based on the XRD data was

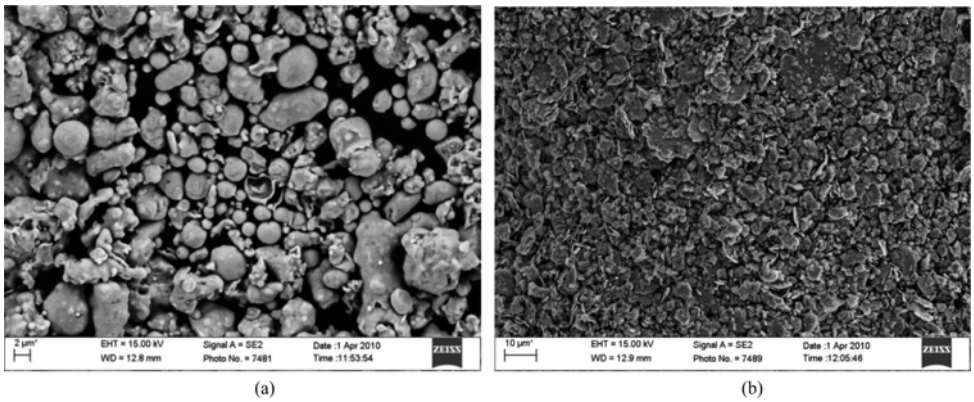

Fig. 2. Morphology of the powders as-atomized (a) and as-cryomilled (b).

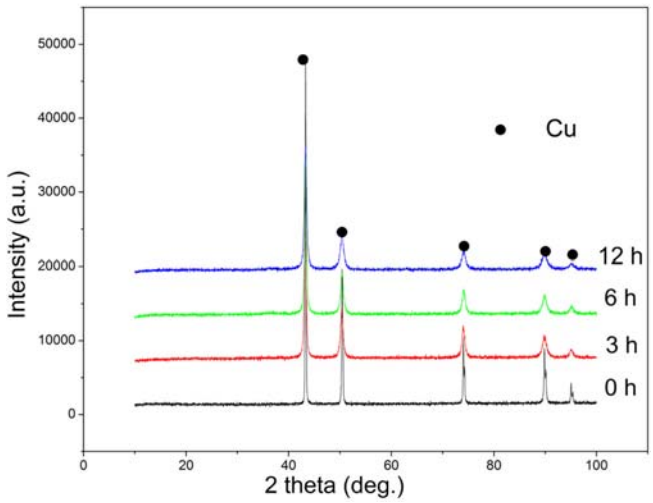

Fig. 4. XRD patterns of cryomilled Cu powders for different milling times.

conducted by the Integral Breadth method, and the grain size values were between 5 nm and 35 nm. This fact may reveal the formation of nanocrystalline structure in the cryomilled powders.

The bright TEM image in Fig. 5(a) shows that the observed fragments had reached the nanoscaled grain size in dimension. The selected area diffraction pattern of the cryomilled powder, shown as a ring pattern in Fig. 5(b), also validates this fact. The phases computed based on the d-spacing from the ring pattern are also shown in Fig. 5(b). Rings corresponding to Cu_2O were also observed, along with those of copper. However, it is likely that the content of Cu_2O in the cryomilled powder is quite small, especially since XRD could not detect the presence of this phase, as is shown in Fig. 4. The HRTEM image in Fig. 5(c) shows that the cryomilled Cu powder had reached a nanoscaled grain size, outlined region with a circle. The grain refinement mechanism

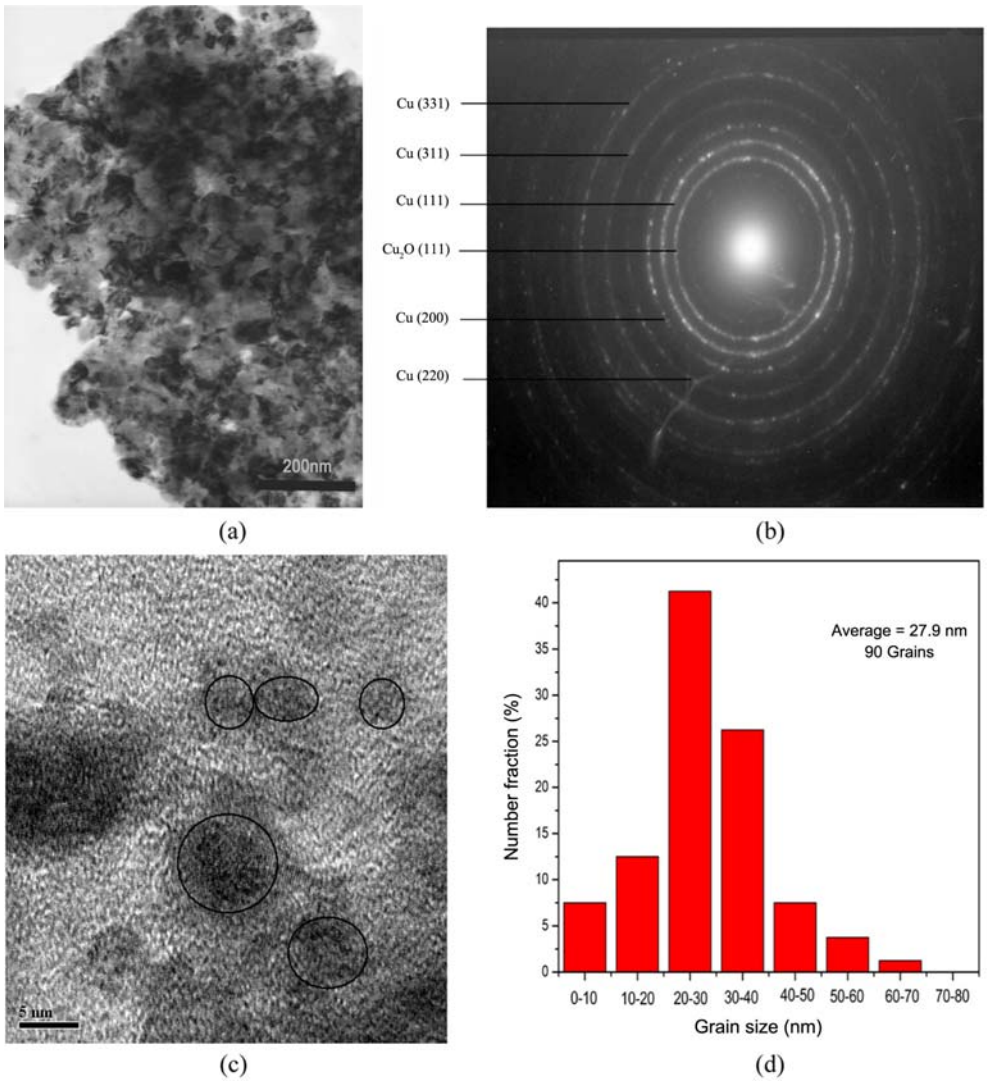

Fig. 5. Bright-field TEM image (a), SAED pattern (b), and HRTEM image (c) of the cryomilled Cu powder, revealing a nanocrystalline grain structure in the powder. (d) The distribution of grains measured from the bright field images.

had three steps during the cryomilling process [3,25]. It started with the localization of the deformation into shear bands with high dislocation density, forming nanometer-scale sub-grains. This sub-grain structure extended throughout the sample during continued milling. The final stage was the transformation of the sub-grain boundary structure to randomly oriented high-angle grain boundaries [25]. At last, these high-angle grain boundaries transformed to nanocrystalline grains, as show in Fig. 5(a). The grain size distribution measurements from the TEM bright field micrographs are presented in Fig. 5(d) and show an average grain size of 27.9 nm. The microstructure, composed mainly of small nanometer grains that were 5 to 40 nm in size, is shown in Fig. 5(a).

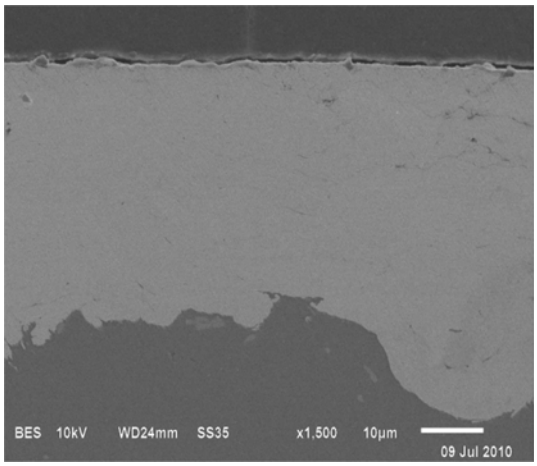

Fig. 6. SEM image of the as-deposited nanocrystalline Cu coating.

3.2. Coating characterization

The typical cross-sectional microstructure of the nanostructured Cu coating analyzed via SEM is seen in Fig. 6. The coating showed excellent interface with the substrate. Cu particles experienced severe deformation, resulting in a relatively low porosity in the coating with irregular surface observed, as shown in Fig. 6. The thickness of the coating was about 100 to 150 µm. It could be considered that the

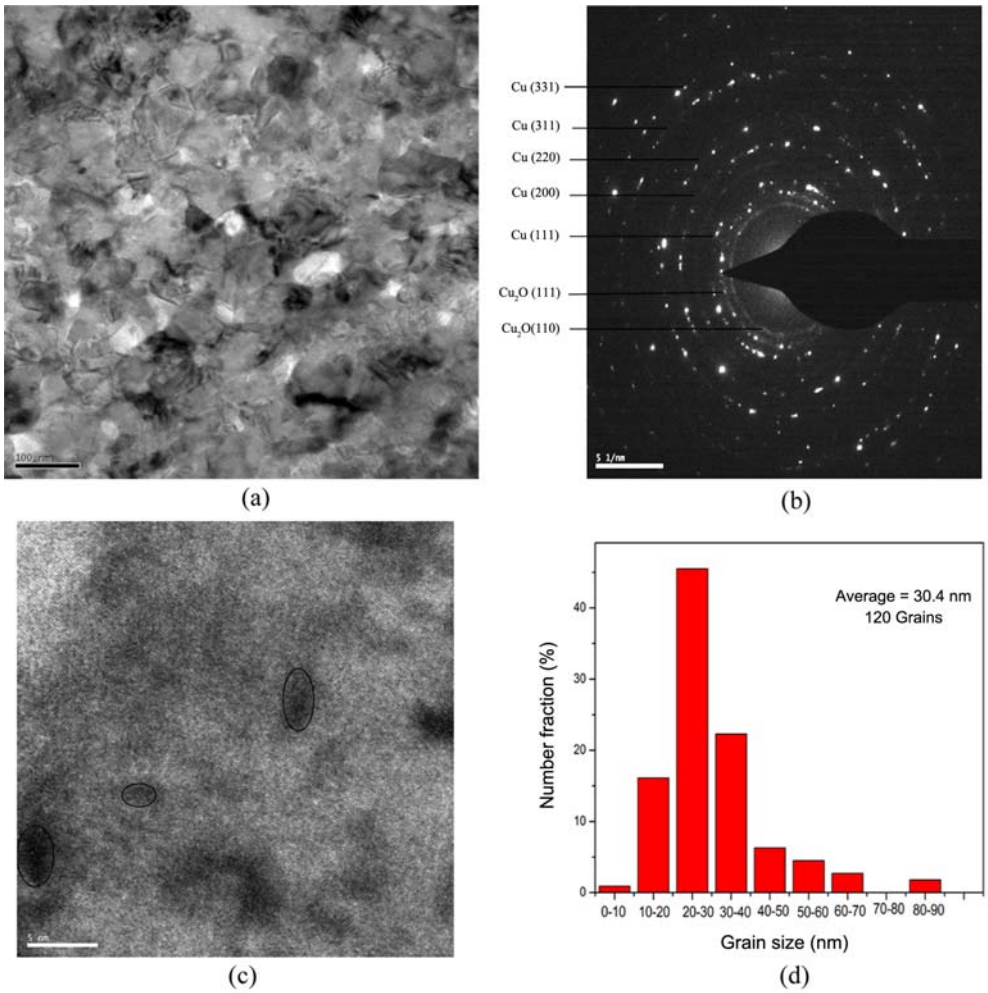

Fig. 7. Bright-field TEM image (a), SAED pattern (b), and HRTEM image (c) of the cold sprayed Cu coating, revealing a nanocrystalline grain structure in the coating. (d) The distribution of grains measured from the bright field images.

high velocity impact of the particles led to densification.

The TEM and HRTEM images in Fig. 7 show that the nanostructured microstructure of the cryomilled powders was retained after the cold spraying process. The samples consisted of grains of irregular shape and random orientation, with an average size of 5 to 40 nm, as shown in Fig. 7(a), in agreement with the XRD results. The corresponding SAED pattern in Fig. 7(b) shows fairly uniform rings, indicating a continuous and wide distribution of misorientations among the nanograins. A close examination of the phases computed based on the d-spacing from the ring pattern also shows the rings corresponding to Cu_2O, along with those of copper, as can be seen in Fig. 7(b). This observation corroborated the result of the aforementioned discussion about the cryomilled Cu powders. It is indicated that high density dislocations were generated throughout the microstructure in the coating, as shown in Fig. 7(c). The grain size distribution measurements from the TEM bright field micrographs are presented in Fig. 7(d) and show an average grain size of 30.4 nm. The microstructure, composed mainly of small nanometer grains that were 5 to 45 nm in size, is shown in Fig. 7(a).

It should be noted that in the 150 micrometers thick coating sample, some of the contaminations introduced during the cryomilling process and during cold spray processing (such as oxygen) could not be excluded, although no other phase has been identified from the electron diffraction pattern except for that of pure fcc Cu. The extremely fine grains might be stabilized by the contaminations. Small amounts of impurity elements (O, N, Fe, etc.) were introduced into the copper matrix during cryomilling processing, with some of them forming nanoscale dispersions. These second phases, in combination with grain boundary segregation of the solute and/or impurity elements, were considered to play a significant role in stabilizing the microstructure [4,41].

3.3. Mechanical behavior

Typical relationship curves of load and hardness versus indentation depth from nanoindentation experiments of the nanostructured and conventional Cu coatings are vividly portrayed in Fig. 8. The measured microhardness of the conventional Cu coating was 1.7 GPa, which was nearly half of the microhardness of the nc Cu coating. The measured microhardness of the cold sprayed nc Cu coating was as high as 3.3 GPa, which was the highest hardness for all the known pure Cu materials, nc or otherwise, which were prepared via other, different approaches. For example, the hardness of the liquid-nitrogen temperature magnetron sputtering (LTMS) Cu sample with d = 10 nm was as high as 3.02 GPa [42]. The hardness of the surface mechanical attrition treatment (SMAT) Cu and the equal channel angular pressing (ECAP) Cu hardness were about 1.75 GPa and 1.67 GPa, respectively [43,44].

The hardness deduced from the analysis of the unloading curves exhibited higher values and should be treated as the

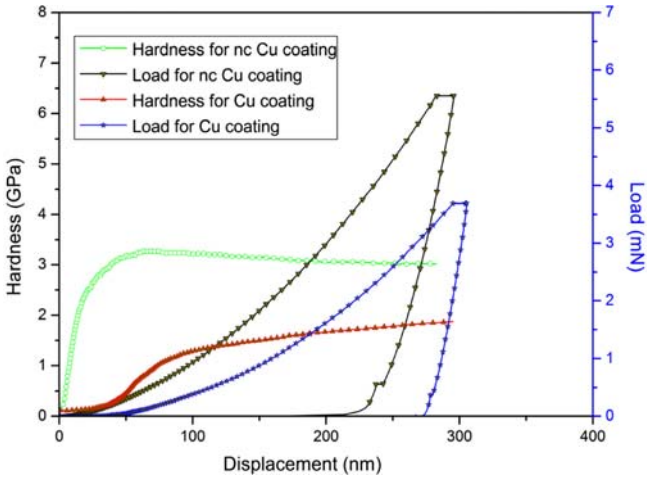

Fig. 8. Load and hardness vs. indentation depth curves for the nanocrystalline and conventional Cu coatings.

mechanical properties of the test material. The higher microhardness can be attributed to the refinement of the grain structure in the nanometer scale and can be rationalized via the Hall-Petch equation [42], assuming the relation:

$$\sigma_y = \sigma_0 + kd^{-\frac{1}{2}} \tag{2}$$

where σ_0 is the friction stress, σ_y is the yield stress, d is the grain size and k is a constant. If the work hardening is not large, the Vickers hardness, Hv divided by 3, usually approximates to the yield strength. Then, the hardness also follows the

Hall-Petch relation:

$$H_v = H_0 + k'd^{-\frac{1}{2}} \tag{3}$$

which relation is applicable for most materials. The Hall-Petch propensity of increasing hardness with decreasing grain size is still maintained; therefore, the Hall-Petch relation is suitable for the hardness variation in the present study.

A close examination of the shape of the measured hardness-displacement curves reveals that the hardness variation had different mechanisms for nc Cu coating and conventional Cu coating. The conventional Cu coating exhibited a propensity of increasing hardness slightly with increasing of the displacement. However, the nanocrystalline Cu coating exhibited an unusual plastic behavior. The curve shows three plastic regimes: work hardening, a narrow domain of plastic yielding at constant flow stress, and work softening with increasing strain. The same behavior, with work hardening and work softening effects, have also been observed by other researchers [45].

One possible explanation for this discrepancy lies in the deformation micromechanisms. At the incipient stage, notice-

able strain hardening effects resulting from grain boundary sliding occurred; these boundaries were saturated by non-equilibrium dislocations. The plastic yielding platform formed as a result of a balance between the strain hardening and the recovery mechanism, including annihilation of dislocations by grain boundaries and grain boundary sliding; continued deformation effectively leads to further dislocation coalescence and favors recovery due to the smaller grain size. At this point, work softening occurs. This is unlike the case of the conventional Cu coating, in which the dislocations in the grain can impede dislocation movement, leading to dislocation interactions and tangling everywhere. And, thus, a work hardening effect occurred.

Other studies have also showed that cold sprayed nc Ni coatings and nc 5083 aluminum coatings had superior mechanical properties and minimal microstructural changes after the cold spraying process [26,28]. Based on these findings, one can indicate that the cold spray method could be an excellent technique for fabricating nc coatings and deposits from nanostructured powders.

4. CONCLUSIONS

Copper powder was cryomilled for 12 hours to generate flake-like powder particles that had particle size in the range of 2 μm to 25 μm. The grain sizes of the cryomilled Cu powder were in the range of 5 to 40 nm.

Nanocrystalline copper coatings were fabricated via cold spraying for the first time. The coating showed negligible porosity and an excellent interface with the substrate. The nanostructured microstructure of the cryomilled powders was retained after the cold spraying process. The severe deformation of the original particles and little evidence of porosity were observed. To the best of our knowledge, the microhardness of the cold sprayed nanocrystalline Cu coatings is as yet the highest hardness value.

The work suggests that the combination of cryomilling and cold spraying techniques is a viable means of fabricating metallic nanostructured coatings with excellent properties for scientific and engineering applications.

ACKNOWLEDGMENTS

The authors wish to acknowledge the financial support provided by the National Natural Science Foundation of China under grants No. 50874009 and No. 50871019; we would also like to thank senior engineer Zhi Lin for helpful discussions about the analysis of nanoindentation data, and Lingyong Cao and Saijie Mou for their help.

REFERENCES

1. H. Gleiter, *Prog. Mater. Sci*. **33**, 223 (1989).
2. M. A. Meyers, A. Mishra, and D. J. Benson, *Prog. Mater. Sci*. **51**, 427 (2006).
3. D. B. Witkin and E. J. Lavernia, *Prog. Mater. Sci*. **51**, 1 (2006).
4. E. J. Lavernia, B. Q. Han, and J. M. Schoenung, *Mater. Sci. Eng.* **493**, 207 (2008).
5. J. H. He and J. M. Schoenung, *Mater. Sci. Eng.* **336**, 274 (2002).
6. A. Papyrin, V. Kosarev, S. Klinkov, A. Alkhimov, and V. Fomin, *Cold Spray Technol.*, p. 1, Elsevier Science, Amsterdam (2007).
7. V. K. Champagne Jr., *The Cold Spray Materials Deposition Process*, p. 1, Woodhead Publishing, Cambridge (2007).
8. G. Bae, Y. M. Xiong, S. Kumar, K. Kang, and C. H. Lee, *Acta Mater.* **56**, 4858 (2008).
9. G. Bae, S. Kumar, S. H. Yoon, K. Kang, H. Na, H. J. Kim, and C. H. Lee, *Acta Mater.* **57**, 5654 (2009).
10. P. C. King, G. Bae, S. H. Zahiri, M. Jahedi, and C. H. Lee, *J. Thermal Spray Technol*. **19**, 620 (2010).
11. G. Bae, K. Kang, J. J. Kim, and C. H. Lee, *Mater. Sci. Eng. A* **527**, 6313 (2010).
12. G. Bae, K. Kang, H. Na, J. J. Kim, and C. H. Lee, *Surf. Coat. Technol*. **204**, 3326 (2010).
13. Y. Zou, W. Qin, E. Irissou, J. G. Legoux, S. Yue, and J. A. Szpunar, *Scr. Mater.* **61**, 899 (2009).
14. S. Kumar, G. Bae, and C. H. Lee, *Appl. Surf. Sci*. **255**, 3472 (2009).
15. K. Spencer and M.-X. Zhang, *Scr. Mater.* **61**, 44 (2009).
16. J. Cho, J. Kim, S. Y. Hwang, and C. H. Lee, *Rev. Adv. Mater. Sci*. **18**, 50 (2008).
17. S. H. Yoon, H. J. Kim, and C. H. Lee, *Surf. Coat. Technol*. **200**, 6022 (2006).
18. S. H. Yoon, Y. M. Xiong, H. Kim, and C. H. Lee, *Appl. Phys*. **42** , 1 (2009).
19. S. H. Yoon, G. Bae, Y. M. Xiong, S. Kumar, K. Kang, J. J. Kim, and C. H. Lee, *Acta Mater* **57**, 6191 (2009).
20. K. Spencer, D. M. Fabijanic, and M.-X. Zhang, *Surf. Coat. Technol*. **204**, 336 (2009).
21. H. J. Kim, D. H. Jung, J. H. Jang, and C. H. Lee, *Mater. Sci. Forum* **534**, 441 (2007).
22. H. Na, G. Bae, S. Shin, S. Kumar, H. J. Kim, and C. H. Lee, *Compos. Sci. Technol*. **69**, 463 (2009).
23. L. Ajdelsztajn, B. Jodoin, G. E. Kim, and J. M. Schoenung, *Metall. Mater. Trans. A* **36**, 657 (2005).
24. P. Richer, B. Jodoin, L. Ajdelsztajn, and E. J. Lavernia, *J. Thermal Spray Technol*. **15**, 246 (2006).
25. L. Ajdelsztajn, A. Zúñiga, B. Jodoin, and E. J. Lavernia, J. *Thermal Spray Technol*. **15**, 184 (2006).
26. A. C. Hall, L. N. Brewer, and T. J. Roemer, *J. Thermal Spray Technol*. **17**, 352 (2008).
27. W.-Y. Li and C.-J. Li, *Appl. Surf. Sci*. **256**, 2193 (2010).
28. L. Ajdelsztajn, B. Jodoin, and J. M. Schoenung, *Surf. Coat. Technol*. **201**, 1166 (2006).
29. R. S. Lima, J. Karthikeyan, C. M. Kay, J. Lindemann, and

C. C. Berndt, *Thin Solid Films* **416**, 129 (2002).
30. C.-J. Li, G.-J. Yang, P.-H. Gao, J. Ma, Y.-Y. Wang, and C.-X. Li, *J. Thermal Spray Technol*. **16**, 1011 (2007).
31. P. Sudharshan Phani, V. Vishnukanthan, and G. Sundararajan, *Acta Mater.* **55**, 4741 (2007).
32. S. R. Bakshi, V. Singh, K. Balani, D. G. McCartney, S. Seal, and A. Agarwal, *Surf. Coat. Technol.* **202**, 5162 (2008).
33. Y.-M. Xiong, K. Kang, S. H. Yoon, and C. H. Lee, *J. Nanosci. Nanotechnol*. **8**, 5561 (2008).
34. J. S. Cheng, H. Cui, H. B. Chen, B. Yang, J. Z. Fan, and J. S. Zhang, *J. Univ. Sci. Technol*. **14**, 523 (2007).
35. H. Cui, K. Tao, X. L. Zhou, and J. S. Zhang, *Rare Met.* **27**, 418 (2008).
36. K. Tao, X.-L. Zhou, H. Cui, H.-B. Chen, Y.-B. Li, and J.-S. Zhang, *Int. J. Min. Met. Mater.* **16**, 77 (2009).
37. Z. Zhang, F. Zhou, and E. J. Lavernia, *Metall. Mater. Trans. A* **34**, 1349 (2003).
38. J. Milligan, R. Vintila, and M. Brochu, *Mater. Sci. Eng. A* **508**, 43 (2009).
39. X. D. Li and B. Bhushan, *Mater. Charact*. **48**, 11 (2002).
40. C. A. Schuh, *Mater. Today* **9**, 32 (2006).
41. V. L. Tellkamp, A. Melmed, and E. J. Lavernia, *Metall. Mater. Trans. A* **32**, 2335 (2001).
42. J. Chen, L. Lu, and K. Lu, *Scr. Mater.* **54**, 1913 (2006).
43. Y. M. Wang, K. Wang, D. Pan, K. Lu, K. J. Hemker, and E. Ma, *Scr. Mater.* **48**, 1581 (2003).
44. R. Z. Valiev, I. V. Alexandrov, Y. T. Zhu, and T. C. Lowe, *J. Mater. Res*. **17**, 5 (2002).
45. Y. Champion, S. Guérin-Mailly, J.-L. Bonnentien, and P. Langlois, *Scr. Mater.* **44**, 1609 (2001).